BioResearch Open Access
Volume 2, Number 1, February 2013

DOI: 10.1089/biores.2012.0286

Bioengineering the Liver: Scale-Up and Cool Chain Delivery of the Liver Cell Biomass for Clinical Targeting in a Bioartificial Liver Support System

Eloy Erro,[1] James Bundy,[1] Isobel Massie,[1] Sherri-Ann Chalmers,[1] Aude Gautier,[1] Spyridon Gerontas,[2] Mike Hoare,[2] Peter Sharratt,[3] Sarah Choudhury,[1] Marcin Lubowiecki,[1] Ian Llewellyn,[1] Cécile Legallais,[4] Barry Fuller,[5] Humphrey Hodgson,[1] and Clare Selden[1]

Abstract

Acute liver failure has a high mortality unless patients receive a liver transplant; however, there are insufficient donor organs to meet the clinical need. The liver may rapidly recover from acute injury by hepatic cell regeneration given time. A bioartificial liver machine can provide temporary liver support to enable such regeneration to occur. We developed a bioartificial liver machine using human-derived liver cells encapsulated in alginate, cultured in a fluidized bed bioreactor to a level of function suitable for clinical use (performance competence). HepG2 cells were encapsulated in alginate using a JetCutter to produce $\sim 500\,\mu$m spherical beads containing cells at ~ 1.75 million cells/mL beads. Within the beads, encapsulated cells proliferated to form compact cell spheroids (AELS) with good cell-to-cell contact and cell function, that were analyzed functionally and by gene expression at mRNA and protein levels. We established a methodology to enable a ~ 34-fold increase in cell density within the AELS over 11–13 days, maintaining cell viability. Optimized nutrient and oxygen provision were numerically modeled and tested experimentally, achieving a cell density at harvest of >45 million cells/mL beads; $>5\times10^{10}$ cells were produced in 1100 mL of beads. This process is scalable to human size ($[0.7–1]\times10^{11}$). A short-term storage protocol at ambient temperature was established, enabling transport from laboratory to bedside over 48 h, appropriate for clinical translation of a manufactured bioartificial liver machine.

Key words: alginate encapsulation; fluidized bed bioreactor; HepG2 cells

Introduction

Acute liver failure can lead to death via a syndrome including hepatic encephalopathy and cerebral edema, multiorgan failure, and sepsis.[1] Rapid and unpredictable progression inhibits timely identification of donor organs for transplantation. We describe a bioartificial liver (BAL) to provide support after liver injury, buying time either to allow organ procurement for transplantation or for natural regeneration to occur.

Liver-assist devices comprise artificial and bioartificial types.[2] Artificial devices use physical/chemical gradients and adsorption to detoxify patients' blood. BAL devices use living cells to replace the complex repertoire of metabolic, synthetic, and detoxifying liver function. Current designs include hepatocytes in flat plate monolayers, within hollow fiber cartridges, in or on other inorganic matrices and encapsulated cells in perfused beds or suspended in scaffolds.[3–15] BAL design criteria include optimized environments for hepatocyte viability and function, bidirectional mass transfer between the blood/plasma and cells, minimum dead volume, and adequate cell numbers. Since normal adult human liver contains $(1–2)\times10^{11}$ hepatocytes, we estimated that $(0.7–1)\times10^{11}$ cells constitute an appropriate biomass (30%–50% of normal), based on minimum liver mass compatible with life (10%–15% after liver resection)[16]; however, biomass has to perform in the hostile environment of liver failure plasma.

[1]Liver Group, UCL Institute of Liver & Digestive Health, and [5]Cell, Tissue & Organ Preservation Unit, University Department of Surgery, UCL Medical School, Royal Free Hospital Campus; [2]The Advanced Center for Biochemical Engineering, Department of Biochemical Engineering; University College London, London, United Kingdom.
[3]PNAC Facility, Department of Biochemistry, University of Cambridge, Cambridge, United Kingdom.
[4]CNRS UMR 6600 Biomechanics and Bioengineering, University of Technology of Compiègne, Compiègne, France.

Many BALs (e.g., hollow-fiber cartridge-based systems) insert molecular barriers between cells and patient circulation, reducing mass transfer. Cell encapsulation in alginate, a biocompatible semipermeable hydrogel that is directly exposed to patients' plasma, provides an alternative technology, protecting cells from shear-stress during perfusion, promoting 3-dimensional culture conditions, and maximizing cell performance.[17,18] We combined this with fluidized bed perfusion technology to maximize mass transfer. The cyclic microgravity environment established between vertical media-flow and the gravity of the alginate-encapsulated liver spheroids (AELSs) maximizes diffusion of metabolites between cells and perfusate. This allows rapid cell growth and spheroid formation, and, when applied clinically, maximizes exchange between biomass and patient plasma.

Alginate is a linear copolymer polysaccharide of covalently (1-4)-linked β-D-mannuronate (M) and α-L-guluronate (G) residues extracted from brown algae. The M and G residue sequence (e.g., homopolymeric M or G blocks or alternating M and G monomers) dictates viscosity and gelling properties of different alginate solutions. A medium-viscosity hydrogel provides a platform within which three-dimensional (3D) spheroidal biomass structures can grow and approximate physiological tissue architecture. AELSs exhibit better growth and up-regulated liver-specific functions compared to monolayer culture, with typical cell architecture demonstrating desmosomes, tight junctions and microvilli, high representation of endoplasmic reticulum and mitochondria, and generation of extracellular matrix reminiscent of that in normal liver.[18]

Potential cell sources for BALs include primary hepatocytes, established cell-lines, and stem cells. Although primary human hepatocytes initially possess the full complement of liver-specific functions, in culture they do not proliferate and rapidly lose differentiated function; they are difficult to obtain due to donor organ scarcity. Porcine hepatocytes have been used clinically in BALs, with the only controlled trial showing no benefit[19] and potential biohazards existing.[20–22] Cells cultured from stem cells offer exciting future prospects, but due to complexity and costs remain impractical at this time. We report here on the use of a well-differentiated human liver–derived cell line (HepG2) isolated from a hepatoblastoma that exhibits many liver-specific functions in monolayer culture,[23] which can be further enhanced by specific culture techniques, such as 3D culture.

Key to clinical feasibility of any BAL is timely delivery to the patient. As BALs will be applied in the unpredicted emergency of acute liver failure, a means of storing performance-competent beads for use as needed is required. We previously demonstrated that encapsulated cells in beads can be cryopreserved;[24] functional recovery of thawed beads on a large scale is as yet insufficient for BAL application. An alternative is short-term storage at ambient temperature, and in this study we developed an oxygen carrier–based method for short term (up to 48 h) AELS preservation, a time-frame suitable for delivery from a central production facility and appropriate clinical use.

We optimized conditions for growing AELSs to performance-competent cell spheroids at a scale suitable for a large animal trial, and their short-term preservation, using combined mathematical modeling and iterative experimentation. While our approach was in order to further the production of a BAL, the system is adaptable to optimize production of other cell lines for therapeutic or manufacturing purposes.

Materials and Methods

Monolayer cell culture to provide seed cells for alginate encapsulation

HepG2 cells (ECACC Wiltshire) were grown using 500-cm^2 tissue culture flasks[17] and modified MEM-alpha media (Gibco) supplemented with fetal calf serum (10%, PAA), insulin (0.27 IU/mL, Novo Nordisk), penicillin/streptomycin (50 μg/mL, PAA), and fungizone (1 mg/mL, PAA), to provide $(5–6)\times10^9$ cells for encapsulation.

Alginate encapsulation

HepG2 cells in culture media were mixed 1:1 with Alginate (2% w/v alginate, medium viscosity [Sigma Aldrich], in 0.015 M HEPES-buffered physiological saline, pH 7.4) yielding $(1.5–1.75)\times10^6$ cells/mL of solution. As a density modifier, 0.0175 g/mL 10- to 50-μm glass beads (Kisker) were added, establishing the appropriate microgravity environment when fluidizing.[25,26]

Beads were made using a JetCutter (GeniaLab). A stainless-steel vessel containing the stirred cell suspension was pressurized to achieve jet flow through a 350-μm nozzle at 20 ± 1 mL/min, cut into segments mechanically by a wire cutting-disc rotating at 3300 rpm. These segments formed droplets on propulsion into polymerization solution (0.204 M $CaCl_2$ in 0.15 M NaCl); collections did not exceed 1 h. The polymerization bath was supplemented with 70% w/v concentrated $CaCl_2$ to replace Ca^{2+} ions sequestered during the gelation process. Subsequently, excess calcium was removed by three washes with Dulbecco's modified Eagle's medium (DMEM; PAA) containing 10% fetal bovine serum, antibiotics, and fungizone. Beads were collected on a 200-μm mesh, and placed in a fluidization chamber for microgravity biomass culture.

Culture of encapsulated cells

The fluidized bed bioreactor (FBB) hosting cell proliferation during the growth phase of the biomass, comprised a 15-L Fermentor (Fermac360, Electrolab), a 30-L reservoir, and a fluidization chamber.[27,28] The chamber and fermentor were connected with 4.8-mm bore silicone tubing (Altec). Media perfusion was achieved (flow rate 180–350 mL/min) with a peristaltic pump (Watson-Marlow). The cell-containing alginate beads were fluidized to a bed-height of 1.56 ± 0.1 fold expansion (mean $\pm$ SD, $n=9$). Beads to culture-media volume ratio was kept at 1:58, with 25%, 50%, 70%, and 80% media replaced on days 4, 6, 8, and 10. Temperature (37°C) and pH (7.4) were maintained by the fermentor during the growth phase; CO_2 and O_2 were supplied through proportional–integral–derivative dynamic control, with design parameters to ensure oxygen levels did not drop below critical levels. Therefore, oxygen saturation in the culture medium was maintained between 15%–35%, avoiding adverse effects of hypoxia or hyperoxia on cell proliferation. During the latter part of the growth phase, additional oxygen was supplied directly inside the chamber, to ensure oxygen saturation was maintained throughout the bed under the high metabolic demand of the proliferating cells. Alpha MEM was

supplemented with glucose to ~24 mM, and 10% human plasma (National Blood Service) was added in place of fetal bovine serum during fermentation. Five amino acids (phenylalanine, cysteine, leucine, isoleucine, methionine) were supplemented to maintain their original media concentration, replenishing that consumed by the biomass.

Samples of media and beads throughout the experiment determined cell function, viability, cell proliferation, glucose consumption, and lactate synthesis. After 11 days of culture AELSs were harvested and prepared for an animal preclinical trial (publication submitted).

Cell viability

One milliliter of beads ($n=5$) containing cells were washed twice in phosphate-buffered saline (PBS; Lonza) and stained using 0.0128 mg/mL fluorescein diacetate (FDA) and 0.0256 mg/mL propidium iodide (PI) vital dyes, and viability was quantified under fluorescence microscopy using Lucia Imaging software, as described.[24]

Cell number

Beads were washed twice in Hank's balanced salt solution. Cell spheroids were liberated from alginate with 16 mM EDTA, pH 7.4, pelleted, resuspended in PBS and disaggregated using a 23-G needle followed by automated cell nuclei quantitation (Nucleocounter, Sartorius-Stedim).

Lactate production and glucose consumption

Lactate production and glucose consumption were quantified by enzyme-linked oxygen-rate measurement using a GM-7 Micro-Stat analyzer (Analox) with a Clark-type amperometric oxygen electrode.

Synthetic function

Protein synthesis was monitored by measurement of alpha-fetoprotein (AFP) release as this specific protein of HepG2 cells is not present in the fresh frozen plasma (FFP) that comprises 10% of the culture media. AFP was measured by sandwich enzyme-linked immunosorbent assay (standards from Applichem), with primary and secondary AFP antibodies (Abcam ab10071 + ab10072).

Gene expression and protein arrays

RNA was prepared from AELSs at the time of optimal cell function and compared with RNA prepared from the same number of monolayer cells. Microarray analysis was performed after first and second strand cDNA synthesis, biotin labeling of mRNA targets with *in vitro* transcription, and cRNA fragmentation to 35–200 base targets, using an Affymetrix U95Av2 human genechip. Relevant genes that showed significant changes were further interrogated by Western blotting and, where possible, functional analysis. Protein lysates (8 mg) were also prepared from these two cell conditions (encapsulated vs. monolayer) and subjected to immunoanalysis using the Powerblot antibody-array (Becton Dickinson), and investigation of protein oxidation using the OxyBlot™ kit (Chemicon International) detecting carbonyl groups (aldehydes and ketones) on proteins that occur at and modify the side chains of lysine, arginine, proline, or threonine residues and form cysteine disulfide bonds as a result of several types of oxidative damage. The carbonyl groups in the protein side chain were derivatized to 2,4-dinitrophenylhydrazone (DNP-hydrazone) by reaction with 2,4-dinitrophenylhydrazine (DNPH) and separated by polyacrylamide gel electrophoresis, followed by Western blotting. Oxidized proteins were revealed by an anti-DNP antibody and quantified on a scanning densitometer.

Bead dimensions

AELSs (250 μL) were washed twice in PBS and loaded onto 2-mm-deep slides. Phase contrast images (Lucia Image Software at 4× magnification) captured ~80–100 beads. Total alginate bead volume was calculated from measured average bead-diameter, and cell-density data. The fraction of beads occupying a determined space (solid-phase porosity: ε_S) compared to media fraction (liquid-phase porosity: ε_L) was empirically estimated by establishing volume of liquid phase (V_{liquid}), total volume including the beads (V_{total}), using the relationships, $\varepsilon_L = V_{liquid}/V_{total}$ and $\varepsilon_S = 1 - \varepsilon_L$.

Biomass preservation

After the proliferation phase, AELSs were stored at ambient temperature for 48 h in sealed T175 culture flasks with perfluorodecalin (PFC; F2 Chemicals) and culture medium. PFC was autoclaved and oxygenated prior to use by bubbling 100% oxygen for 10 min; media contained 25 mM HEPES, pH 7.4 (Invitrogen, 15630). To develop optimal conditions for ambient storage, AELSs were stored at different ratios of PFC/culture media with different headspace volumes. An antioxidant mixture comprising 0.85 mM Trolox (Sigma, 238813), 500 IU/mL Catalase (Sigma, c9322) and 3 mM N-acetyl cysteine (Sigma, a8199) was trialed for efficacy.

Amino acid concentration

Concentrations of essential amino acids in the medium were measured serially and sampled during the fermentation phase and at the end of the PFC storage to explore depletion.

Media samples were protein depleted and homogenized; 5 nmol norleucine (internal standard) and loading buffer (60 μL) were added to 10 μL of sample, which was then injected onto an amino acid analyzer (Biochrom 30). Ion-exchange chromatography (sodium system) eluted amino acids with a series of buffers over pH 3.2–6.45 range. Peak detection was achieved by mixing the eluate with ninhydrin at 135°C and measuring absorbance at 570 and 440 nm. Quantitation used Chromeleon software and calibration curves for each amino acid.[29]

Statistics

Analysis of variance and Student's *t*-test assessed significance of data (Excel, GraphPad Prism), and mean ± SEM or SD is reported.

Results

Cell growth and viability in 3D environment

HepG2 cells were cultured in the alginate matrix under a fluidized regime. A cell density of $(46.57 \pm 6.3) \times 10^6$ cells/mL of alginate bead at harvest (mean ± SEM, $n=5$) was

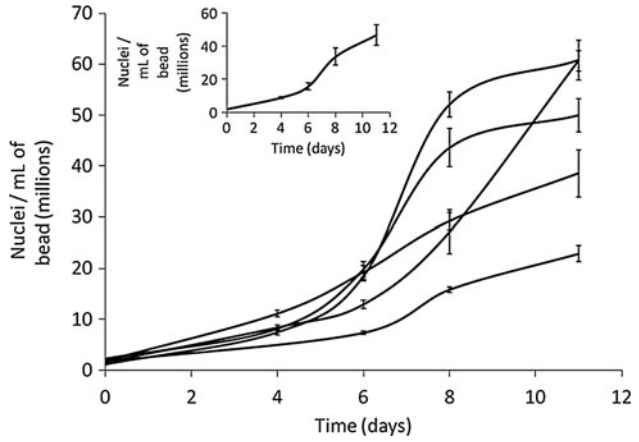

FIG. 1. Cell density in beads during proliferation phase of the biomass ($n=5$, mean ± SEM). *Inset*: Average proliferation, $(46.57 \pm 6.3) \times 10^6$ cells/mL at harvest (SEM).

achieved over the growth phase (Fig. 1), a total biomass of $(5.43 \pm 0.7) \times 10^{10}$ cells (SEM, $n=5$). Media supplementation with human FFP promoted high cell proliferation, and later, differentiated liver function during 11 days' cultivation. A transient decrease in viability assessed by propidium iodide was recorded immediately after encapsulation (viabilities at 83.44 ± 6.2%). By day 1 (less than 24 h after encapsulation) viability increased to >93% (93.85% ± 2.3%), a small but significant difference ($p<0.05$). This is likely to reflect a transient alteration in membrane integrity since in contrast in 24 h the total number of cells visualized had not changed; day 0: 2.44 ± 0.4 and day 1: $(1.94 \pm 0.1) \times 10^6$ nuclei/mL, $p=0.08$, nor had the viable cell number, $p>0.3$. Figure 2 reflects the viability after encapsulation and at harvest on day 11.

Biomass performance

Glucose concentration decreased over time, despite interventional glucose supplementation, but was maintained >15 mM over the exponential growth period (Fig. 3A). Glucose consumption rate, expressed as micromoles per million cells per day, decreased over the proliferation period (14.3 ± 7.96 on day 4; 6.43 ± 2.09 on day 6; 9.01 ± 2.76 on day 8; mean ± SEM, $n=5$). By harvest, consumption dropped to 2.87 ± 0.54 (mean ± SEM, $n=5$), concomitant with the decrease in proliferation. Lactate accumulated in the culture medium, consistent with the metabolic profile of this cell line (Fig. 3B).[30] Lactate build-up was minimized by media replacement on days 4, 6, 8, and 10. Sustained AFP production was observed over the proliferation period (Fig. 3C).

Gene and protein expression

RNA microarrays and protein powerblot arrays indicated alginate-encapsulated cells expressed cytoprotective pathways to a greater extent than monolayer-cultured cells. Thus, protein oxidation measured by Western blotting of protein carbonyl groups (OxyBlot™), indicated protection by alginate-encapsulation and culture ($n=2$): (monolayer 26.1 and 35.5 vs. AELS 9.27 and 7.86 densitometric units). When stressed by hypoxia and reperfusion, this protection persisted (monolayer 43.47 and 46.14 vs. AELS 24.16 and 30.24). Heat-shock protein 70 (HSP70), catalase, and MHC class I were increased in AELS cf. monolayers by 3.46-, 2.44-, and 3.2-fold, respectively, at mRNA levels, while HSP47 and RNA polymerase II were decreased by 3.15- and 2.38-fold, respectively. By Western blotting MAPKp49 (8.36 vs. 9.75) and ST1/Hop-p60 (7.70 vs. 13.99) were decreased in AELSs while p38delta was unchanged cf. monolayer; these data were confirmed by Powerblot array. Hemoxygenase 1 (HO-1) was dramatically increased in AELSs (13.37 vs. 5.50) while HO-2 was unchanged (2.89 vs. 2.98). The Powerblot array was further interrogated for adaptive- and cellular-stress proteins (Table 1) demonstrating increases in eight and decreases in two proteins associated with adaptive stress, and an increase in cathepsin D29, a protein involved in tissue remodeling. CDC42, a Rho protein that activates the protein kinase MEKK1 was decreased as was HSF4-38, a heat-shock factor that mediates the transcription of heat-shock proteins when HSP70 or 90 are decreased. This provides more confidence in the

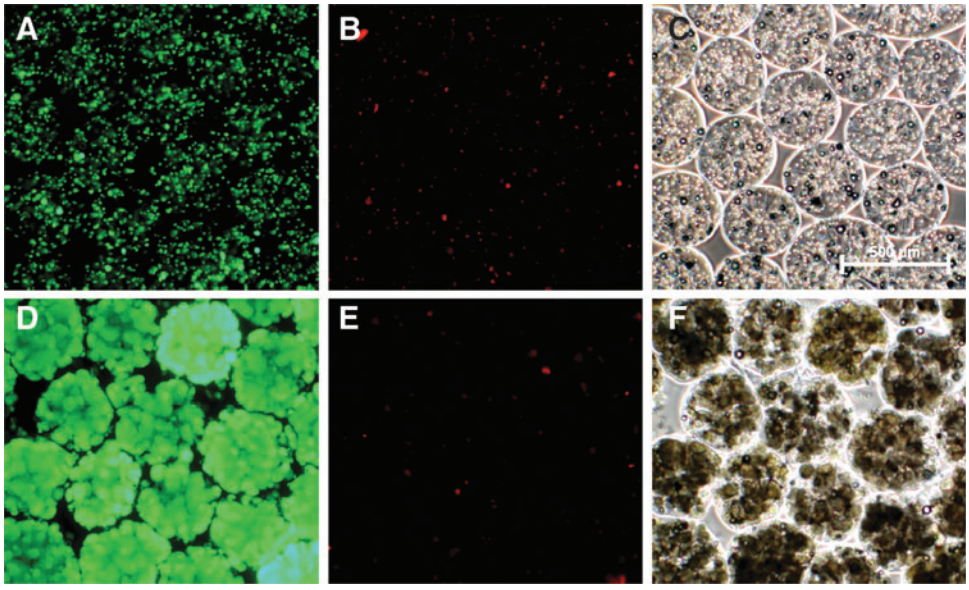

FIG. 2. Viability and phase contrast microscopy of HepG2s encapsulated in alginate beads. **(A, D)** Fluorescein diacetate (FDA)-stained viable cells. **(B, E)** Propidium iodide (PI)-stained dead cells. **(C, F)** Phase contrast images. **(A–C)** Day of encapsulation, **(D–F)** after 10 days of proliferation in fluidized bed bioreactor.

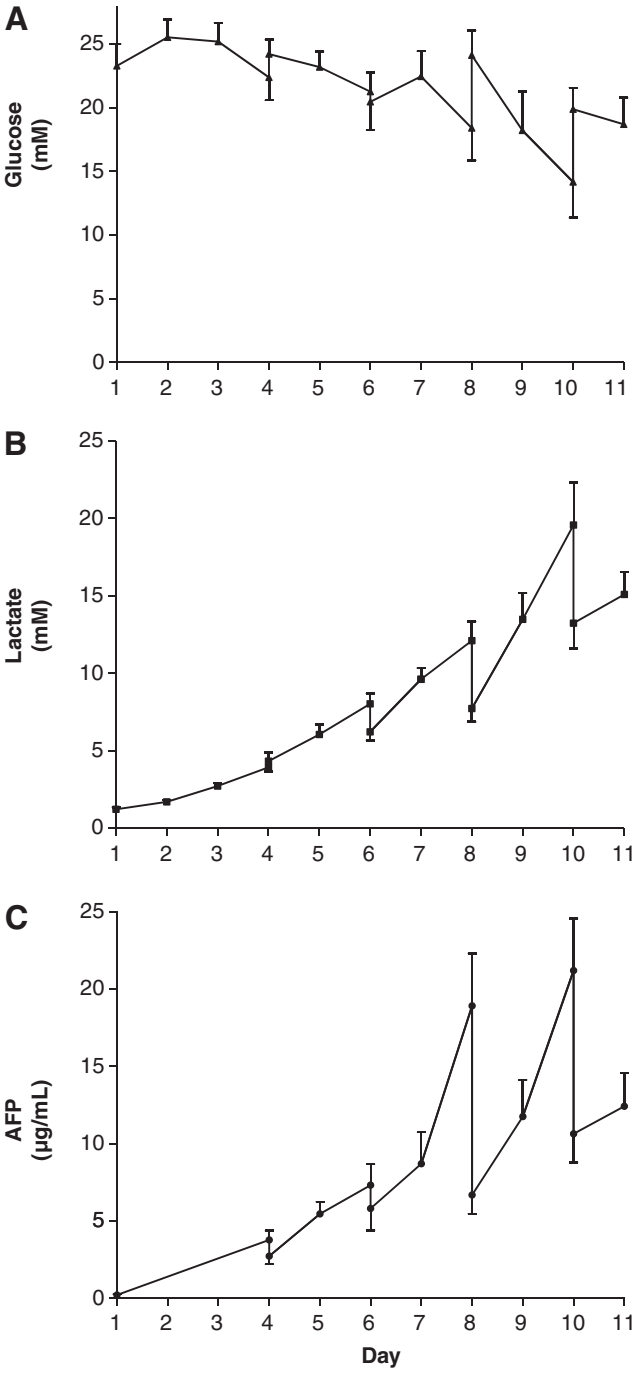

FIG. 3. Metabolite levels during culture of proliferating biomass. **(A)** Glucose concentration during proliferation phase ($n=5$, mean ± SEM), peaks match media changes on days 4, 6, 8, and 10). **(B)** Lactate profile: Lactate concentration during proliferation ($n=5$, mean ± SEM). Falls in lactate correspond to media changes (days 4, 6, 8, and 10). **(C)** Alpha-fetoprotein (AFP) concentration; vertical lines represent samples before and after media change.

microarray data, which showed an increase in HSP70. Catalase specific activity was increased: AELS 18 ± 1 mU/min per mg of protein vs. monolayer 8 ± 1 mU/min per mg of protein.

There were increases in two cell cycle–associated proteins; KAP-27, a cdk-associated phosphatase cell cycle regulator by 3.55-fold, and NBS1, a part of the DNA repair/telomere length maintenance mechanism by 2.67-fold. Five proteins were decreased: Bub3 cl.31, 3.46-fold; GCAP-1, 6.74-fold; NEK2-46, 2.71-fold; IAK1-46, 2.68-fold; and cyclin-B, 2.26-fold. Proliferation was assessed immunocytochemically using antibodies to endogenous Ki67 and to exogenously added BRDU. Staining was evident throughout the liver cell spheroids, in ~50% of the cells, irrespective of their position within the spheroid; moreover, there were no necrotic centers, as assessed by hematoxylin and eosin (HE) staining (data not shown).

Nutrient provision

Amino acid levels over 12 days in the bioreactor media initially showed a marked decline in five essential amino acids: leucine, isoleucine, cystine, methionine, and phenylalanine, despite regular medium changes. All but cystine had dropped below 60% of the starting concentration by day 6 and continued to decline, with phenylalanine being totally consumed on days 9 and 11. These data informed a mathematical model, predicting amino acid consumption of AELSs during fermentation; this was fine-tuned via iterative empirical measurements. Figure 4A shows data for all amino acids whose concentration fell during the proliferation stage of biomass culture. After establishing the maximum concentration that could be used without toxicity to the cells for each (Supplementary Fig. S1), leucine, isoleucine, cysteine, methionine, and phenylalanine were added daily from a stock concentration of 100 mM, thus maintaining these key depleted amino acids (Fig. 4B) at ≥60% of initial levels.

Alginate bead physical parameters.

Average bead size after encapsulation was 528 ± 69.6 μm (mean ± SD, $n=558$) and after harvest 566 ± 74 μm (mean ± SD, $n=473$; no significant difference). The average number of cells per bead immediately after encapsulation was 320 ± 30.4 (mean ± SEM, $n=5$) and 10,868 ± 1971 (men ± SEM, $n=5$) at harvest—an approximately 34-fold increase in cells/bead. There were ~4400 beads per milliliter of biomass. Beads occupied 42% of the total volume (ε_S) when settled.

Oxygen consumption

Dissolved oxygen (DO) levels during cell proliferation were measured in the reservoir (probe: DO1) and also downstream of the biomass (probe: DO2), measuring oxygen depletion by proliferating cells and controlling oxygenation by increasing DO setpoint. To prevent hyperoxic toxicity to biomass, oxygen delivery at the inlet to the growth chamber was ≤35%. Additional oxygen was supplied directly within the growth chamber by a thin membrane oxygenator. Figure 5 illustrates the oxygenation parameters and consumption of a representative experiment.

Biomass preservation at room temperature

Preliminary data showed a lack of headspace (air) above the AELS suspension in cell flasks resulted in poor AELS viability even after PFC supplementation. Increasing headspace to 50% improved viability to >80%. When AELS to medium ratio was 1:1, viability was 80%, improving to 95% when the volume of medium was increased to 10 times that of beads

Table 1. Powerblot Analysis

	Catalog or product no.	Confidence level	Fold change	Function
Adaptive stress proteins				
p115	P67420	5	+2.09	Vesicular transport from the ER to Golgi
Plectin −144	P92020	5	+3.04	Filament binding protein-crosslinking in cytoskeleton
E-cadherin	C377020	5	+1.98	Calcium-dependent adhesion molecule; increase reduces invasive carcinoma, important for epithelial junction formation
Fibronectin	F14420	5	+4.03	Extracellular matrix protein via integrin binds to collage and attachment to cell, cellular signaling
HSP60	H99020	4	+2.01	Heat shock protein (HSP), constitutively expressed in normal and apoptotic cells
Annexin IV	A29920	4	+2.44	Family of calcium and phospholipid binding proteins
Adaptin alpha	A43920	4	+2.21	Recruits membrane proteins, vesicular transport
REF-1	R64820	4	+2.51	Redox factor. Increase by AP-1 DNA binding, DNA repair
HRF	H42020	5	−6.37	Histamine releasing factor
Nip-1	N79420	4	−1.95	Pro-apoptotic proteins, target proteins to mitochondria
Cellular stress response protein				
Cathepsin D-29	C47620	5	+9.2	Tissue remodeling in response to estrogen
CDC42	C70820	5	−4.3	Rho protein, activates MEKK1
HSF4 –38	H65520	5	−4.25	Heat shock factor, mediates transcription of HSPs, increases when there is a decrease of HSP70, 90
Cell cycle proteins				
KAP-27	K32120	4	+3.55	Cdk-associated phosphatase, cell cycle regulation
NBS1	N10720	4	+2.67	Nijmejin breakage syndrome-complex with Rad 50 and MRE11, important for both DNA damage and repair, and telomere length maintenance
Bub3 cl.31	B11520	5	−3.46	Sensing kinetochore attachment to microtubules during prometaphase to metaphase transition
GCAP-1	G54220	4	−6.74	Guanylate cyclase binding protein, cell cycle progression
NEK2-46	N52120	4	−2.71	Nima related kinase, conditions, controls entry of cells into S phase and mitosis
IAK1-46	I71320	4	−2.68	Mammalian chromosome segregation

The most significant results are shown, grouped into biological functions. Confidence levels 5 and 4 are shown as most significant, as a result of reproducibility of results and fold increases. Stress proteins increased in three-dimensional (3D) cultures cf. monolayer culture suggesting an adaptive response to enhanced performance. Comparison of cell-cycle proteins in AELS vs. monolayer, showing that the majority of cell-cycle proteins decreased, since doubling time of monolayer HepG2 cells increased from ~24 h to 2–3 days when proliferating in 3D culture.

with an antioxidant cocktail. Viable cell numbers improved by approximately 23% over 48 h compared with control. Essential amino acid concentrations at the end of storage were all sufficiently high, except for valine. The chosen optimized protocol for bead to media to PFC ratio was 1:10:1, headspace was 50%, antioxidants and valine (1.965 mM) added. Cell viability was maintained (85.4% ± 12.3%; mean ± SD, $n=9$ after 48 h; compared to a starting value of 93% ± 8.1%; mean ± SD, $n=9$; no significant difference, $p>0.05$), and proliferation continued during storage such that viable cell numbers were not decreased.

Discussion

The clinical imperative

To date only organ transplantation successfully replaces the failed human liver. Controlled clinical trials of bioartificial liver and artificial liver devices have not shown improved survival. A review from Carpentier et al.[31] summarized the bioartificial device data, while two artificial device trials based on albumin dialysis have been more recently reported.[32,33] The justification for providing temporary liver support derives both from current surgical practice and extensive animal work, which have repeatedly demonstrated that there is a critical mass of liver that is required for survival. Currently this is exemplified by "small for size" liver scenarios that affect both resectional surgery for tumors and living-donor liver transplantation; in these cases insufficient liver mass may be present postsurgery for adequate liver function and greater confirmed functional biomass would clearly be of considerable value.

Our hypothesis is that HepG2 cells cultured in an optimized form can replace deficient liver function adequately to allow adequate time for liver repair to take place or to buy time for an organ donor to be identified.

Fulfilling the functional requirements

In vitro data indicate that these cells do express a panel of Phase I and Phase 2 detoxifying enzymes when cultured in 3D format in our system (AELSs), although at a lower level than primary cells. Additionally, they metabolize ammonia, and they produce new transport proteins, notably albumin.

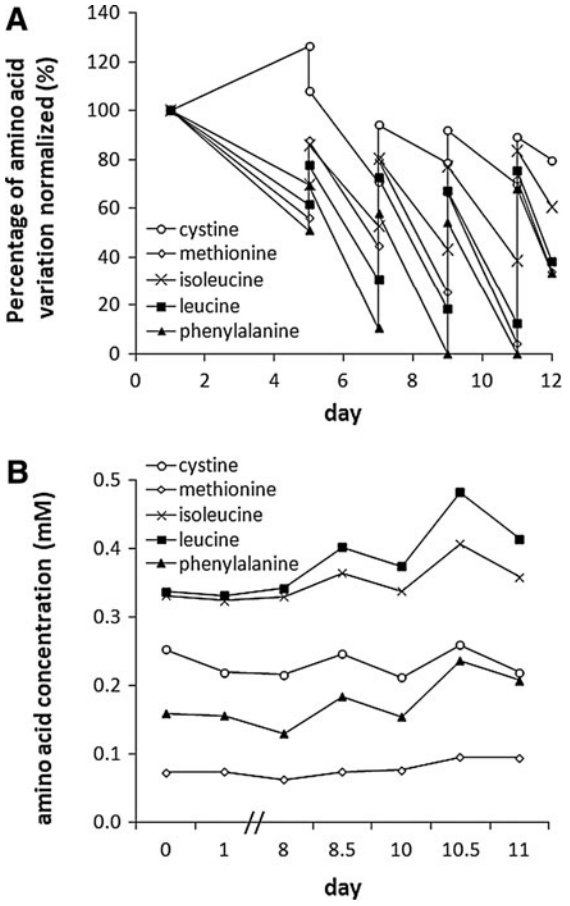

FIG. 4. Amino acid levels during biomass production. **(A)** Amino acid levels during 12 days of biomass cultivation. Graph shows consumption of five key amino acids being only partially replenished by media changes on days 5, 7, 9, and 11. **(B)** Successful maintenance of depleted amino acids during fermentation. Control was by use of a model relating cell proliferation and amino acid consumption to predict media supplementation; in all cases the minimum amino acid concentrations remained above 60% of initial value.

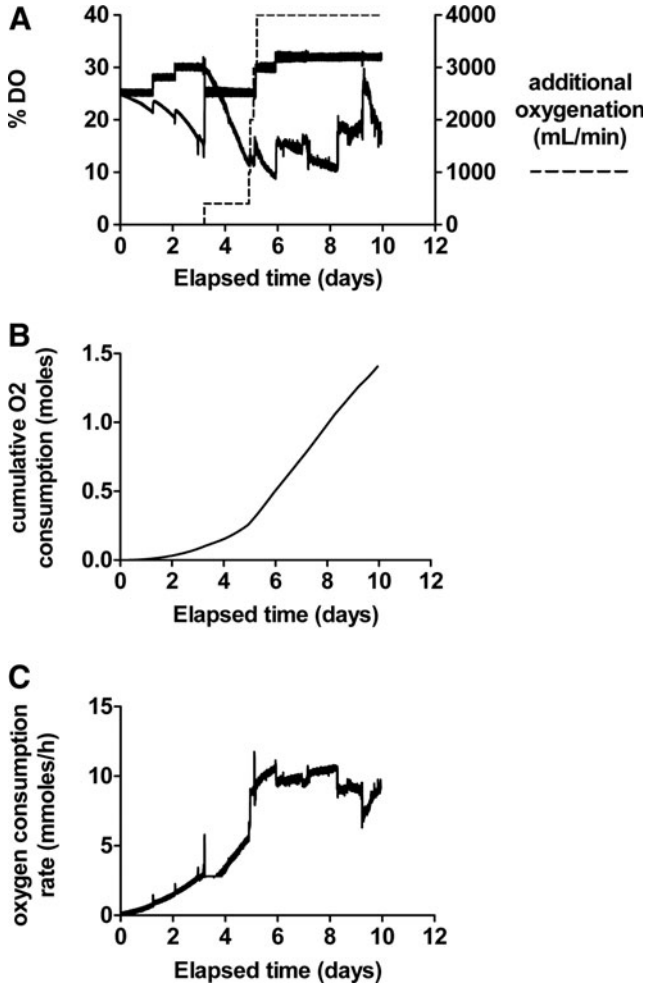

FIG. 5. Oxygenation of a typical fluidized bed bioreactor experiment over 11 days. **(A)** Dissolved oxygen (DO)1 (dO_2 in fermentor), DO2 (dO_2 immediately after the biomass); additional oxygenation (dashed line) supplied directly to the biomass chamber. **(B)** Cumulative oxygen consumption of biomass. **(C)** Oxygen consumption in millimoles per hour.

Clearly each individual metabolic detoxifying pathway above is likely to be supplemented proportionately to the number of cells over which a patient's plasma is perfused.

The provision of freshly synthesized albumin also merits note. In particular, many nonbiological liver machine studies are based on a form of albumin dialysis. While none so far has improved survival, there is symptomatic relief in some patients, which is associated with the removal of certain toxins by the albumin. However, an issue that has clearly emerged is the source and thus biological efficacy of the albumin in such systems, and its fitness-for-purpose as a carrier protein to aid detoxification. Commercially isolated or prepared albumin has an altered affinity for toxins that makes it considerably less effective than native albumin; the loss of function being attributed in part to the preservatives (e.g., cacodylate) used in their preparation. An advantage of our system is that the HepG2 cells are continuously making endogenous nascent albumin and indeed, we have demonstrated that in our system the per cell production is equivalent to that calculated from human *in vivo* data. This nascent albumin has obviously never been exposed to preservatives or other manufacturing processes that adversely affect the toxin-binding characteristics of commercial albumin.

Providing adequate functioning biomass requires innovation in cell culture conditions and scale, bioreactor technology, and preservation and transport parameters, and we have addressed all of these.

Physical advantages of the system

Hepatocyte function is affected by cell shape and by the presence of extracellular matrix. Alginate has many advantages as an exogenous matrix, being a natural product harvested globally to commercial scale and being relatively bio-inert, with purified preparations nonantigenic in the patient.[34,35] Its semipermeable nature in the polymerized form provides a protective environment and a structure for cell growth and adherence suitable for epithelial cells. As a 1% hydrogel (i.e., 99% fluid),[26] it allows ready release of cell-synthesized substances into the surrounding milieu, and

free passage of small molecules through the gel to the cells. We described elsewhere the favorable effects when cells are encapsulated in alginate, generating 3D colonies of polarized cells with excellent morphology, locally generated extracellular matrix proteins, and up-regulated functionality.[17,36–39] Encapsulation, using the JetCutter technology we describe, allows efficient production of a cell mass adequate to charge a bioreactor for human use in <3 h, convenient and feasible for industrial production. Calcium ion concentration is critical during encapsulation and culture. This affects polymerization via covalently bonding adjacent alginate chains, modulating permeability, size, shape, and rigidity of the beads. Calcium is also hygroscopic and can cause bead swelling, but our technique of stabilizing calcium concentrations resulted in stable bead size, indicating bead integrity throughout encapsulation and culture.[40]

Alginate encapsulation minimizes shear stress to cells,[41] advantageous in the context of a fluidized bed perfusion system. The fluidizing motion does not affect mechanical strength of alginate beads.[25] Feasibility of an FBB based on alginate beads was proven by mathematical modeling and empirical testing[27] using encapsulated cells immediately after encapsulation without prior culture. Here we extended that approach to include prolonged culture allowing cell proliferation, development of cell-to-cell contacts, and the critical benefits of 3D culture increasing per cell performance over time. The microgravity, rather than static regime also up-regulates per cell functionality.[36]

The choice of biomass

Using HepG2 cells in BALs has caused controversy. They are a tumor cell line, albeit derived from a well-differentiated hepatoblastoma. Notably one clone derived from the original cell line has been used in an FDA-approved clinical trial in man.[15] We previously referred to the known deficiencies in some hepatic functions (e.g., absent functional ornithine transcarbamylase in the urea cycle),[42] although other pathways of ammonia assimilation are present. HepG2 cells have two modes of amino acid transport, the mode used by primary hepatocytes (System N) and that used by tumor cells (System ASC, sodium-dependent amino acid transporter) resulting in rapid glutamine uptake several fold faster than primary hepatocytes alone—offering an explanation of how ammonia, incorporated into glutamine, may be lowered by this system.[43,44]

Further, other detoxifying functions, such as those associated with cytochrome P450 enzymes, when up-regulated by the 3D culture compared with monolayer culture, rise to levels within the lower quartile of cultured primary human hepatocytes.[45] We and others have identified many genes that are up-regulated in 3D culture compared with monolayer.[46–48] Some metabolic pathways appear even more favorable than primary hepatocytes for use in a BAL; for example, ATP generation from aerobic glycolysis in the presence of adequate oxygen and normal mitochondria[49] may confer an advantage in liver failure plasma since such metabolically switched cells are resistant to xenobiotics and to compounds causing mitochondrial uncoupling and dysfunction. Moreover, synthetic, detoxifying functions and viability were maintained after perfusion for 6–8 h in liver failure plasma in previous work.[37]

The microarray data presented here indicate that HepG2 cells cultured in alginate beads demonstrate adaptive and potentially beneficial stress responses.[50] Catalase and glutathione-S-transferase, both involved in antioxidant defense[51,52] were increased, and stress-inducible phosphoprotein ST1/Hopp60 decreased. Expression of the molecular chaperone HSP70 increased, potentially preventing denaturation of existing cellular proteins and promoting the initial folding of nascent proteins.[53,54] Another cytoprotective pathway, HO-1,[55] was increased in AELSs. Moreover, a decrease in lipid peroxidation and protein oxidation in encapsulated cells suggests the milieu within the alginate polymer reduced cellular stress associated with increased function.

It has been estimated that between 10% and 30% of the liver cell mass is sufficient for adequate replacement of liver activity.[56] Previous BALs may have failed partly due to an underestimation of the required cell numbers for liver support.[16] Here we demonstrated the expansion of HepG2 numbers to a level suitable for use in an animal trial and demonstrate that the processes described regularly generates 40–50 billion cells 25%–50% of that in normal adult liver,[57] in an alginate scaffold occupying less than 1700 cm^3, with high cell viabilities.

Achieving these cell numbers required a protocol to address nutrient deficiency, toxic chemical build-up, and metabolite diffusion in the bioreactors. Mass transfer models were coupled with Monod kinetics to describe oxygen diffusion and cell proliferation. Oxygen diffusivity values are derived from Gerontas et al.[58]; oxygen uptake rates are derived from fluidized bed experimental data. Regions of high oxygen level (DOT = 35%) seen at the base of the vessel drop to ~8% DOT in region of biomass, increasing again in upper cell-free zone, thus at all times exceeding the levels seen in areas of venous draining (lowest oxygen) in the liver. Our oxygen consumption on a per cell basis compares favorably at 0.038 fmol/sec per cell with those data derived from the AMC bioreactor (0.0166 fmol/sec per cell) [59] and even more so from the hollow fiber cartridge charged with primary human hepatocytes from Mueller et al.[60] at 0.0028 fmol/sec per cell. Depletion of the five most required amino acids was adequately prevented by intermittent supplementation regimes based on modeling or iterative experimental confirmation; this approach is simpler, reduces cost, and is more readily applicable in bioreactor technology than would be large-scale complete media changes.

Biochemical studies monitoring metabolism suggested sequential change during progression of the AELSs cultured over time. The rise in glucose concentration during days 1–2 is consistent with gluconeogenesis by hepatic cells, before proliferation enters the log-phase and glucose consumption increases; a later fall in consumption towards the end of culture suggests a change from a proliferative toward a more differentiated phenotype. AFP production similarly changed over time; production of this protein is characteristic of less-differentiated hepatocytes, cf. normal mature adult hepatocytes, which preferentially produce albumin. AFP progressively accumulated up to 8 days and then decreased compatible with greater differentiation of the cells. Others have also shown a decrease in AFP production accompanied by albumin secretion on 3D culture of liver cells suggesting a switch from proliferation to differentiation.[61]

The cells are performing aerobic glycolysis in which situation lactate accumulation does not reflect hypoxia. There is no

reason to expect preferential and thus potentially toxic lactate accumulation in the center of the beads (as might be the case in a solid tissue mass) for several reasons. Each bead is only ~500 μm in diameter, with only a 250-μm pathway from surface to center, and is a 1% hydrogel without any outside membrane, such that oxygen will be adequately transferred to the center. Further, HE sections of beads did not show any central necrosis, and proliferation of cells was not diminished in the central area.

Comparison with hollow fiber–based systems

The system described here differs in several respects from the ELAD device, which also used a human liver-derived cell line, C3A, a subclone of HepG2 cells. The major differences between the ELAD device and our system reside in (1) directly facilitated mass transfer between the cells and the patient's plasma, (2) the ability to accurately quantify cell number, viability, and function, both synthetic and metabolic, in the biomass to provide validation for the bioartificial liver, and (3) the improved per cell performance the alginate-encapsulated liver cells demonstrate. ELAD uses a hollow fiber cartridge charged with C3A cells inoculated on one side of a hollow fiber membrane, with a 100-kDa plasma filtrate passing through the fibers. Even with a plasma filtrate, the high protein concentration of plasma is likely to cause a degree of membrane fouling and pore blockage. This is in direct contrast to our system using cells encapsulated in a 1% porous hydrogel without a diffusion limiting membrane, perfused by whole plasma, that allows even large molecules such as fibrinogen (MW 340 kDA) to pass freely. Moreover, since each functional unit is a ~0.5-mm diameter bead and each exists in its own milieu of plasma, the degree of mass transfer as a whole is extremely high.[26] We have previously published functional data on AELSs in a BAL format (e.g., bilirubin conjugation, protein synthetic function, glucose consumption)[37] and most recently the preclinical results in a porcine model of ischemic acute liver failure.[62]

Preservation at ambient temperature

Preservation of cells in AELSs during storage and transport to the recipient is a considerable logistical challenge for future clinical application. While successful cryopreservation of performance competent encapsulated liver cells would provide an indefinite shelf life, functional recovery of cryopreserved cells at the clinical scale is not yet sufficient. We therefore developed a protocol for storage of beads at ambient temperature over 48 h as a time useful for transport of the biomass to the bedside. Most recently we successfully used the system, prior to testing in an animal model, to allow transport to a site distant to AELS production.[62] Although metabolism is reduced at mild hypothermia (ambient temperature) compared with 37°C, provision of oxygen is necessary and was achieved by supplementing the AELS suspension with oxygen-saturated PFC, such as is used for oxygen delivery in organ preservation.[63–65] Preservation of function during PFC-supported transport required optimization of headspace to medium ratio, allowing for adequate gaseous exchange, cell-bead to medium ratios, and essential amino acid concentrations. Finally, as hypothermia can result in oxidative stress, known to be damaging to encapsulated liver cells,[66–68] viable cells numbers were improved using antioxidants with this technique.

Viability was successfully maintained for AELSs over 48 h at ambient temperature, and as far as we are aware, it is the first time this approach has been utilized for storage of any encapsulated cells, providing transport of competent beads from GMP production sites to end-user clinics. It may also be applicable for other regenerative medicine applications.

Thus, we developed a scalable system based on a simple, ~0.5-mm-diameter cell-containing bead as the unit of function. The use of a cell-line confers reliability in proliferation; the application of a fluidized bed perfusion enabled good mass transfer, and the system is a straightforward concept with potential for highly complex applications. We have already used this system successfully in a large animal model of acute liver failure in pigs (Supplementary Fig. S2), demonstrating improvement in a number of clinically important parameters of liver function.[62]

Acknowledgments

We thank NIHR, Liver Group Charity, Weston Foundation, Eranda Foundation, Peter Stebbings Memorial Charity, and Steele Charitable Trust.

Disclosure Statement

No competing financial interests exist.

References

1. Ostapowicz G, Fontana RJ, Schiodt FV, et al. Results of a prospective study of acute liver failure at 17 tertiary care centers in the United States. Ann Intern Med. 2002;137:947–954.
2. Carpentier B, Gautier A, Legallais C. Artificial and bioartificial liver devices: present and future. Gut. 2009;58:1690–1702.
3. Gerlach J, Kloppel K, Schauwecker HH, et al. Use of hepatocytes in adhesion and suspension cultures for liver support bioreactors. Int J Artif Organs. 1989;12:788–792.
4. Liu JJ, Chen BS, Tsai TF, et al. Long term and large-scale cultivation of human hepatoma Hep G2 cells in hollow fiber bioreactor. Cultivation of human hepatoma Hep G2 in hollow fiber bioreactor. Cytotechnology. 1991;5:129–139.
5. Matsushita T, Ijima H, Koide N, et al. High albumin production by multicellular spheroids of adult rat hepatocytes formed in the pores of polyurethane foam. Appl Microbiol Biotechnol. 1991;36:324–326.
6. Shatford RA, Nyberg SL, Meier SJ, et al. Hepatocyte function in a hollow fiber bioreactor: a potential bioartificial liver. J Surg Res. 1992;53:549–557.
7. Rozga J, Williams F, Ro MS, et al. Development of a bioartificial liver: properties and function of a hollow-fiber module inoculated with liver cells. Hepatology. 1993;17:258–265.
8. Bader A, Knop E, Frühauf N, et al. Reconstruction of liver tissue in vitro: geometry of characteristic flat bed, hollow fiber, and spouted bed bioreactors with reference to the in vivo liver. Artif Organs. 1995;19:941–950.
9. Naruse K, Sakai Y, Nagashima I, et al. Comparisons of porcine hepatocyte spheroids and single hepatocytes in the non-woven fabric bioartificial liver module. Int J Artif Organs. 1996;19:605–609.
10. Flendrig LM, la Soe JW, Jörning GG, et al. In vitro evaluation of a novel bioreactor based on an integral oxygenator and a spirally wound nonwoven polyester matrix for hepatocyte culture as small aggregates. J Hepatol. 1997;26:1379–1392.

11. Ohshima N, Yanagi K, Miyoshi H. Packed-bed type reactor to attain high density culture of hepatocytes for use as a bioartificial liver. Artif Organs. 1997;21:1169–1176.
12. Matsuura T, Kawada M, Hasumura S, et al. High density culture of immortalized liver endothelial cells in the radial-flow bioreactor in the development of an artificial liver. Int J Artif Organs. 1998;21:229–234.
13. Busse B, Gerlach JC. Bioreactors for hybrid liver support: historical aspects and novel designs. Ann NY Acad Sci. 1999; 875:326–339.
14. Shito M, Kim NH, Baskaran H, et al. In vitro and in vivo evaluation of albumin synthesis rate of porcine hepatocytes in a flat-plate bioreactor. Artif Organs. 2001;25:571–578.
15. Ellis AJ, Hughes RD, Wendon JA, et al. Pilot-controlled trial of the extracorporeal liver assist device in acute liver failure. Hepatology. 1996;24:1446–1451.
16. Starzl TE, Putnam CW, Groth CG, et al. Alopecia, ascites, and incomplete regeneration after 85 to 90 per cent liver resection. Am J Surg. 1975;129:587–590.
17. Khalil M, Shariat-Panahi A, Tootle R, et al. Human hepatocyte cell lines proliferating as cohesive spheroid colonies in alginate markedly upregulate both synthetic and detoxificatory liver function. J Hepatol. 2001;34:68–77.
18. Selden C, Khalil M, Hodgson H. Three dimensional culture upregulates extracellular matrix protein expression in human liver cell lines—a step towards mimicking the liver in vivo? Int J Artif Organs. 2000;23:774–781.
19. Demetriou AA, Brown RS Jr, Busuttil RW, et al. Prospective, randomized, multicenter, controlled trial of a bioartificial liver in treating acute liver failure. Ann Surg. 2004;239: 660–667.
20. Fruhauf JH, Mertsching H, Giri S, et al. Porcine endogenous retrovirus released by a bioartificial liver infects primary human cells. Liver Int. 2009;29:1553–1561.
21. Baquerizo A, Mhoyan A, Kearns-Jonker M, et al. Characterization of human xenoreactive antibodies in liver failure patients exposed to pig hepatocytes after bioartificial liver treatment: an ex vivo model of pig to human xenotransplantation. Transplantation. 1999;67:5–18.
22. Baquerizo A, Mhoyan A, Shirwan H, et al. Xenoantibody response of patients with severe acute liver failure exposed to porcine antigens following treatment with a bioartificial liver. Transplant Proc. 1997;29:964–965.
23. Knowles BB, Howe CC, Aden DP. Human hepatocellular carcinoma cell lines secrete the major plasma proteins and hepatitis B surface antigen. Science. 1980;209:497–499.
24. Massie I, Selden C, Hodgson H, et al. Cryopreservation of encapsulated liver spheroids for a bioartificial liver: reducing latent cryoinjury using an ice nucleating agent. Tissue Eng Part C. 2011;17:765–774.
25. David B, Barbe L, Barthes-Biesel D, et al. Mechanical properties of alginate beads hosting hepatocytes in a fluidized bed bioreactor. Int J Artif Organs. 2006;29:756–763.
26. David B, Dore E, Jaffrin MY, et al. Mass transfers in a fluidized bed bioreactor using alginate beads for a future bioartificial liver. Int J Artif Organs. 2004;27:284–293.
27. Legallais C, Dore E, Paullier P. Design of a fluidized bed bioartificial liver. Artif Organs. 2000;24:519–525.
28. Legallais C, Jaffrin MY. A feasibility study of a filtration type autotransfusion device. J Biomed Eng. 1993;15:143–147.
29. Spackman DH, Stein WH, Moore S. Automatic recording apparatus for use in the chromatography of amino acids. Anal Chem. 1958;**30:**1190–1206.
30. Blackard WG, Clore JN, Powers LP. A stimulatory effect of FFA on glycolysis unmasked in cells with impaired oxidative capacity. Am J Physiol. 1990;259:E451–E456.
31. Carpentier B, Gautier A, Legallais C. Artificial and bioartificial liver devices: present and future. Gut. 2009;58:1690–1702.
32. Rifai K, Kribben A, Gerken G, et al. Extracorporeal liver support by fractionated plasma separation and adsorption (Prometheus®) in patients with acute-on-chronic liver failure (Helios Study): a prospective randomized controlled multicenter study. J Hepatol. 2010;52:S3.
33. Banares R, Nevens F, Larsen FS, et al. Extracorporeal liver support with the molecular adsorbent recirculating system (MARS) in patients with acute-on-chronic liver failure (AOCLF). The Relief Trial. J Hepatol. 2010;52:S459–S460.
34. Menard M, Dusseault J, Langlois G, et al. Role of protein contaminants in the immunogenicity of alginates. J Biomed Mater Res B Appl Biomater. 2010;93:333–340.
35. Klock G, Pfeffermann A, Ryser C, et al. Biocompatibility of mannuronic acid-rich alginates. Biomaterials. 1997;18:707–713.
36. Coward SM, Selden C, Mantalaris A, et al. Proliferation rates of HepG2 cells encapsulated in alginate are increased in a microgravity environment compared with static cultures. Artif Organs. 2005;29:152–158.
37. Coward SM, Legallais C, David B, et al. Alginate-encapsulated HepG2 cells in a fluidized bed bioreactor maintain function in human liver failure plasma. Artif Organs. 2009;33:1117–1126.
38. Damelin LH, Coward S, Kirwan M, et al. Fat-loaded HepG2 spheroids exhibit enhanced protection from pro-oxidant and cytokine induced damage. J Cell Biochem. 2007;101:723–734.
39. Selden C, Shariat A, McCloskey P, et al. Three-dimensional in vitro cell culture leads to a marked upregulation of cell function in human hepatocyte cell lines—an important tool for the development of a bioartificial liver machine. Ann NY Acad Sci. 1999;875:353–363.
40. Thu B, Bruheim P, Espevik T, et al. Alginate polycation microcapsules. II. Some functional properties. Biomaterials. 1996;17:1069–1079.
41. Dore E, Legallais C. A new concept of bioartificial liver based on a fluidized bed bioreactor. Ther Apher. 1999;3:264–267.
42. Mavri-Damelin D, Eaton S, Damelin LH, et al. Ornithine transcarbamylase and arginase I deficiency are responsible for diminished urea cycle function in the human hepatoblastoma cell line HepG2. Int J Biochem Cell Biol. 2007;39: 555–564.
43. Bode BP, Souba WW. Modulation of cellular proliferation alters glutamine transport and metabolism in human hepatoma cells. Ann Surg. 1994;220:411–422.
44. Bode BP, Fuchs BC, Hurley BP, et al. Molecular and functional analysis of glutamine uptake in human hepatoma and liver-derived cells. Am J Physiol Gastrointest Liver Physiol. 2002;283:G1062-G1073.
45. Wilkening S, Stahl F, Bader A. Comparison of primary human hepatocytes and hepatoma cell line HEPG2 with regard to their biotransformation properties. Drug Metab Dispos. 2003;31:1035–1042.
46. Khaoustov VI, Risin D, Pellis NR, et al. Microarray analysis of genes differentially expressed in HEPG2 cells cultured in simulated microgravity: preliminary report. In Vitro Cell Dev Biol Anim. 2001;37:84–88.
47. Shimada M, Yamashita Y, Tanaka S, et al. Characteristic gene expression induced by polyurethane foam/spheroid culture of hepatoma cell line, Hep G2 as a promising cell source

for bioartificial liver. Hepatogastroenterology. 2007;54:814–820.
48. Thomas A, Hodgson HJF, Selden C. Cytochrome P450 activity in HepG2 cells is significantly chemically enhanced and can be maintained in the absence of inducer. BASL 2007;44.
49. Marroquin LD, Hynes J, Dykens JA, et al. Circumventing the crabtree effect: replacing media glucose with galactose increases susceptibility of HepG2 cells to mitochondrial toxicants. Toxicol Sci. 2007;97:539–547.
50. Nilsson HO, Blom J, Abu Al-Soud W, et al. Effect of cold starvation, acid stress, and nutrients on metabolic activity of *Helicobacter pylori*. Appl Environ Microbiol. 2002;68:11–19.
51. Bai J, Cederbaum AI. Adenovirus-mediated overexpression of catalase in the cytosolic or mitochondrial compartment protects against cytochrome P450 2E1-dependent toxicity in HepG2 cells. J Biol Chem. 2001;276:4315–4321.
52. Bai JX, Rodriguez AM, Melendez JA, et al. Overexpression of catalase in cytosolic or mitochondrial compartment protects HepG2 cells against oxidative injury. J Biol Chem. 1999;274: 26217–26224.
53. Papp E, Nardai G, Soti C, et al. Molecular chaperones, stress proteins and redox homeostasis. Biofactors. 2003;17:249–257.
54. Patel B, Khaliq A, JarvisEvans J, et al. Hypoxia induces HSP 70 gene expression in human hepatoma (HEP G2) cells. Biochem Mol Biol Int. 1995;36:907–912.
55. Poss KD, Tonegawa S. Reduced stress defense in heme oxygenase 1-deficient cells. Proc Natl Acad Sci USA. 1997;94: 10925–10930.
56. Allen JW, Hassanein T, Bhatia SN. Advances in bioartificial liver devices. Hepatology. 2001;34:447–455.
57. Imamura H, Kawasaki S, Shiga J, et al. Quantitative evaluation of parenchymal liver cell volume and total hepatocyte number in cirrhotic patients. Hepatology. 1991;14:448–453.
58. Gerontas S, Farid SS, Hoare M. Windows of operation for bioreactor design for the controlled formation of tissue-engineered arteries. Biotechnol Prog. 2009;25:842–853.
59. Poyck PP, Hoekstra R, van Wijk AC, et al. Functional and morphological comparison of three primary liver cell types cultured in the AMC bioartificial liver. Liver Transpl. 2007; 13:589–598.
60. Mueller D, Tascher G, Müller-Vieira U, et al. In-depth physiological characterization of primary human hepatocytes in a 3D hollow-fiber bioreactor. J Tissue Eng Regen Med. 2011; 5:e207–218.
61. Schmelzer E, Triolo F, Turner ME, et al. Three-dimensional perfusion bioreactor culture supports differentiation of human fetal liver cells. Tissue Eng Part A. 2010;16:2007–2016.
62. Selden C, Erro E, Spearman W, et al. Towards a clinical bioartificial liver machine based on human liver cells. Int J Artif Organs. 2012;35(8):555–587.
63. Matsumoto S. Clinical application of perfluorocarbons for organ preservation. Artif Cells Blood Substit Immobil Biotechnol. 2005;33:75–82.
64. Gioviale MC, Damiano G, Palumbo VD, et al. Pancreatic islets from non-heart-beating donor pig: two-layer preservation method in an in vitro porcine model. Int J Artif Organs. 2011;34:519–525.
65. Hosgood SA, Nicholson ML. The role of perfluorocarbon in organ preservation. Transplantation. 2010;89:1169–1175.
66. Vairetti M, Griffini P, Pietrocola G, et al. Cold-induced apoptosis in isolated rat hepatocytes: protective role of glutathione. Free Radic Biol Med. 2001;31:954–961.
67. Huang H, Salahudeen AK. Cold induces catalytic iron release of cytochrome P-450 origin: a critical step in cold storage-induced renal injury. Am. J Transpl. 2002;2:631–639.
68. Karhumaki P, Tiitinen SL, Turpeinen H, et al. Inhibition of ERK 1/2 activation by phenolic antioxidants protects kidney tubular cells during cold storage. Transplantation. 2007;83: 948–953.

Address correspondence to:
Clare Selden, PhD
UCL Institute of Liver & Digestive Health—Liver Group
UCL Medical School
Royal Free Hospital Campus
Rowland Hill Street
Hampstead, London NW3 2PF
United Kingdom

E-mail: c.selden@ucl.ac.uk